

Prospects for a camera-based detector for neutron reflectometry

H. Ambaye (ORNL), T. Charlton (ORNL), S. Flavin (UTK), X. Wen (UTK), M.R. Fitzsimmons
(ORNL&UTK)

We report the outcome of a proof-of-principle (IPTS-29165) neutron reflectivity measurement obtained using a neutron scintillator and a Photonis (brand)^{*} camera. We were motivated to test this technology because it provides much better spatial resolution and count rate capability than the BL4A ^3He position sensitive detector (Table 1). The report describes the detector setup, challenges encountered, a reflectivity measurement and next steps.

Table 1 Bold face are specifications or measurements; italics are derived quantities.

Feature	BL4A detector	Camera
Pixel size	0.8 mm x 0.8 mm	55 μm x 55 μm
Number of pixels	304 by 256	256 x 256
<i>Active detector area</i>	<i>24 cm by 20 cm</i>	<i>1 cm x 1 cm</i>
<i>Field of view</i>	<i>n/a</i>	<i>3 cm x 3 cm[†]</i>
Max count rate (all detector)	1 kHz[‡]	80 MHz
<i>Max count rate/pixel</i>	<i>~10 Hz</i>	<i>1.2 kHz</i>

Detector Setup

The camera was equipped with a lens and light intensifier (Figure 1). The lens was focused on the image of a neutron (LiF:ZnS) scintillator:phosphor[§] measuring ~5 cm by ~5 at a distance of ~10 cm. The image was reflected by a smooth mirror into the camera. The largest lens aperture, i.e., smallest *f*-stop number, was selected. The light intensifier was selected for blue light with variable gain that could achieve single photon detection. Light from the intensifier passed into a TimePix3 chip. The chip consists of an array of 256 by 256 pixels. A pixel has the dimensions of 55 μm by 55 μm .

The camera, mirror and scintillator were housed inside a commercial light-tight box measuring about 24" x 24" x 16" (Figure 1, left). The unit was placed on the detector arm in the region

* <https://www.amsins.com/asi-photonis-joint-venture/>

[†] The field-of-view is determined by the optical properties of the lens. For our application with the lens provided by the manufacturer the field-of-view was 3x3 cm² focused onto a 1x1 cm² chip.

[‡] Per Fitzsimmons and Charlton (*Nuclear Instrumentation and Methods A* **941**, 162330 (2019)).

<https://doi.org/10.1016/j.nima.2019.06.071>), the BL4A detector exhibits 60 Hz noise (not phased to the source) regardless of 30 or 60 Hz operation of the choppers when the count rate integrated over the direct beam (of ~5 by 20 pixels) exceeds 1 kHz.

[§] We tested several scintillators and settled for using the Eljen Technology LiF:ZnS 0.5 mm thick product EJ-426-0-PA <https://eljentechnology.com/products/neutron-detectors/ej-426>. This scintillator absorbed about 82% of $\bar{\lambda} = 5.5 \text{ \AA}$ neutrons and 95% of the $\bar{\lambda} = 11.5 \text{ \AA}$ neutrons.



Figure 1 (left) View inside of light-tight box. (right) Enclosure mounted on the detector arm.

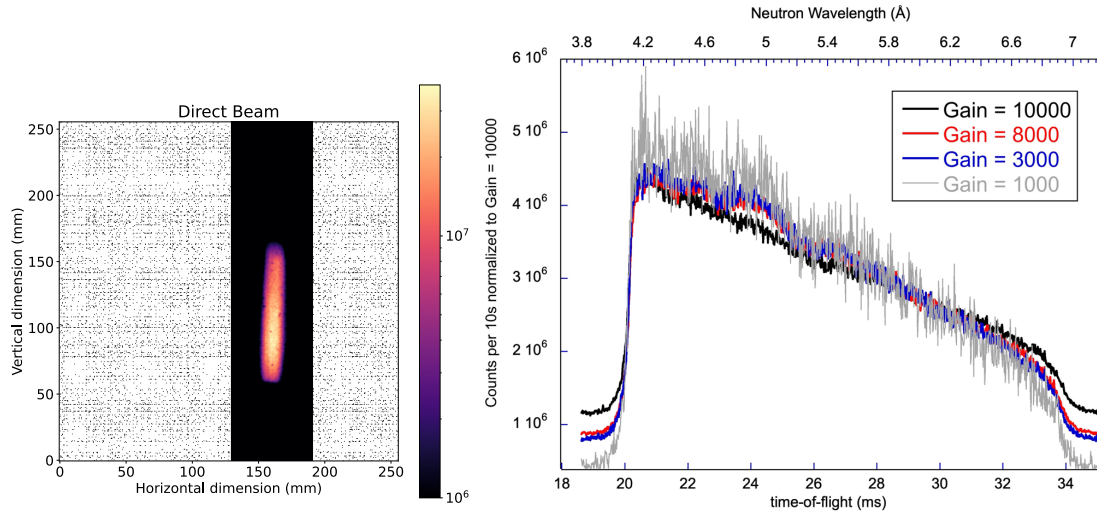


Figure 2 (left) Image of direct beam integrated over all times-of-flight. (right) Variation of spectra vs. time-of-flight for different gain settings. The instrument operated at 60 Hz. The sample to scintillator distance was 0.65 m.

normally supporting the downstream (after-sample) neutron spin flipper (Figure 1, right). Because there is no slit between the sample and the camera box, we installed a Cd mask with a ~3 mm wide slit onto the surface of the scintillator. The Cd mask allowed us to block the direct beam while we observed the specular reflection from the sample. The two beams (one strong and one weak) have different optimal gain settings (the gain is set by a 0-5 VDC power supply 10x gain per volt).

The camera in the BL4A hutch was connected to a Mac laptop in the 4A data cabin via a 10 Gb/s fiber optic cable. A measurement involved setting the incident angle of the sample and detector angle with the BL4A instrument computer, then initiating data collection on the Mac. The first TSYNC signal from the accelerator triggered the shutter to open, and it remained open until the desired collection time was achieved. TSYNC pulses were recorded via the TDC1

metadata channel of the camera. Photon events (intensities, positions and times), henceforth called the event stream, were recorded by the TimePix3 chip. The rising edges from the TDC1 channel and the event stream were recorded with 1 ps accuracy. Spectra of the direct and reflected beams were recorded using different gain settings. We found the largest gain was ideal for the reflected beam, yet too large for the direct beam (which led to distortion of the direct beam spectra for the largest setting only). Importantly, the spectra of the *entire* direct beam as viewed by large slits ($S1H = S2H = S3H = 1$ mm and $S1V = S2V = 25$ mm $S3V = 15$ mm) could be obtained without saturating the detector for modest gain settings (Figure 2). The opportunity to do away with measurements of only fractions of the direct beam improves data quality/reliability and is very attractive. A second attraction is that we *did not observe* any evidence for noise coincident with beam-on-target with the camera. This is unlike the case for the BL4A detector (either or both the camera and scintillator are insensitive to the prompt pulse noise, whatever its origin, e.g., neutron or facility noise). Owing to modest-size elements in the scintillator:phosphor, the material is more sensitive to γ -rays than is the ${}^3\text{He}$ detector (which has some sensitivity owing to the quench gas). Nevertheless, we did not observe any signal from γ -rays, which may be due to the characteristics of BL4A.

Challenges Encountered

Table 2 reports the challenges encountered and solutions executed or proposed.

Table 2 Challenges and solutions (or not).

Issue	Problem	Solution	Problem addressed
Ambient light observed inside the light-tight enclosure	Increases the background of the image	<ul style="list-style-type: none"> Identify source and mitigate Install optical baffles Install high pass optical filter 	No
Rollover of the timing signals for meta and event streams	ps-accuracy leads to rollover of int64 variables about 26s into the measurement. Neutron measurements last much longer.	<ul style="list-style-type: none"> Implemented time corrections in the Jupyter Notebook. ps-accuracy not needed for neutron scattering, explore less, e.g., ns or μs accuracy. 	Yes
10-100Gb data files are unwieldy	<ul style="list-style-type: none"> Loading complete data sets into laptop or MRAC1/2 not possible. 	<ul style="list-style-type: none"> Restricted analysis to a small region of interest; could analyze a 10+Gb file overnight 	Yes

	<ul style="list-style-type: none"> • Calculations of times-of-flight based on difference between meta and event streams are very time consuming (of orders 10's to 100's hours) • Real-time visualization of more than 20-s of data not practical • Difficulty storing data and porting elsewhere • An exposure lasting 2 minutes produces about 10Gb of data 	<ul style="list-style-type: none"> • Stored data on personal 3-Tb drive 	
Phosphor afterglow	The phosphor has a long <i>optical</i> decay time-constant which adversely affects the time-of-flight spectrum.	See discussion	No

A reflectivity measurement

The specular neutron reflectivity of the Pt(40nm)/Ta(20nm)/Al₂O₃ sample (provided by Prof. E. Guo) was obtained for a small range of Q. Shown in Figure 3 (left) is the position intensity of the specular reflection integrated over all time-of-flight after subtraction of background. Figure 3 (right) shows a comparison of the *signal intensity* (not the reflectivity!) integrated over all position vs. time-of-flight obtained from the ³He detector and the camera. Note, the wavelength ranges (not shown) corresponding to the times-of-flight for the two measurements are slightly different due to the difference between the sample-to-detector distances. Both spectra were taken for the same incident beam and detector angles and correspond to Q straddling the critical edge. For long wavelengths beyond the critical edge the spectra vary as the spectrum of the source. The most noticeable difference between the spectra in Figure 3 (right) is the magnitude of the background. Remarkably, the background away from the specular reflection for the camera-measured-data (Figure 2, left) is zero after the usual background subtraction method applied in Module 2 of the Jupyter Notebook code.^{**} This method involves attributing to background the events observed (vs. time-of-flight) in the region

^{**} M.R. Fitzsimmons and T.R. Charlton, *Tools to perform data reduction of time-of-flight data taken on BL4A (MagRef)—a Jupyter notebook approach* (2020). <https://doi.org/10.5281/zenodo.3968838>

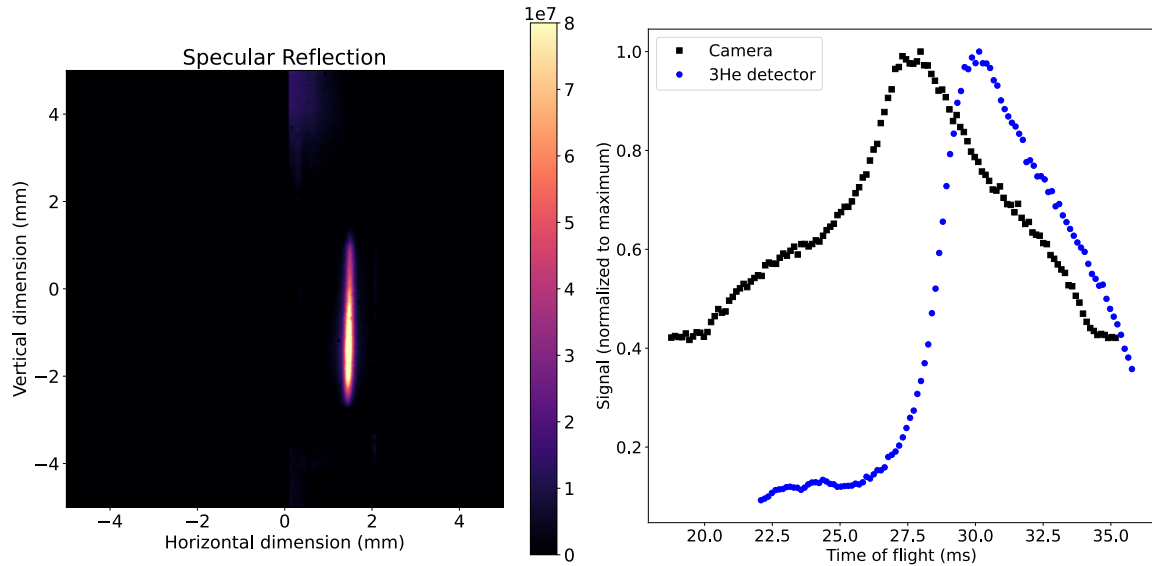


Figure 3 (left) Position image of the specular reflection integrated over all times-of-flight. (right) Signal integrated over all positions of the specular reflection vs. time-of-flight for the ${}^3\text{He}$ detector (blue) and camera (black).

contained within the large box excluding the events contained inside the small box in the example shown in Figure 4. The background is fitted to a simple plane function (vs. time-of-flight) –the fitted function providing an interpolation of the background under the reflection in the smaller box.

The difference of the spectra provides a learning moment. The scintillation portion of the LiF:ZnS is ${}^6\text{LiF}$. The decay time of the scintillation is 200 ns.^{††} Coupled to the scintillator is the ZnS phosphor, which has a much longer (*optical* decay) time constant (or afterglow). To measure the time constant of the phosphor, we exposed the scintillator to the direct beam (see Figure 2, left), then we closed the neutron shutter and recorded two images of the scintillator taken two minutes apart (Figure 5). A region-of-interest was defined including the region of the scintillator exposed to the direct beam and the intensities in these regions integrated. From the ratio of the intensities, we obtained a time constant of 102 s for the afterglow (of the phosphor). Because the afterglow is induced only in the region the neutron beam (specular or otherwise) that strikes the scintillator, the afterglow is contained inside the smaller box of Figure 4, thus, the method to estimate background cannot account for the background due to

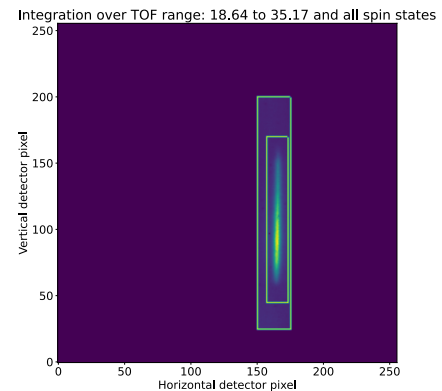


Figure 4 Image showing the small region of interest containing the specular reflection. Events in the region between the two boxes are used to estimate background in the smaller region.

^{††} <https://eljentech.com/products/neutron-detectors/ej-426>

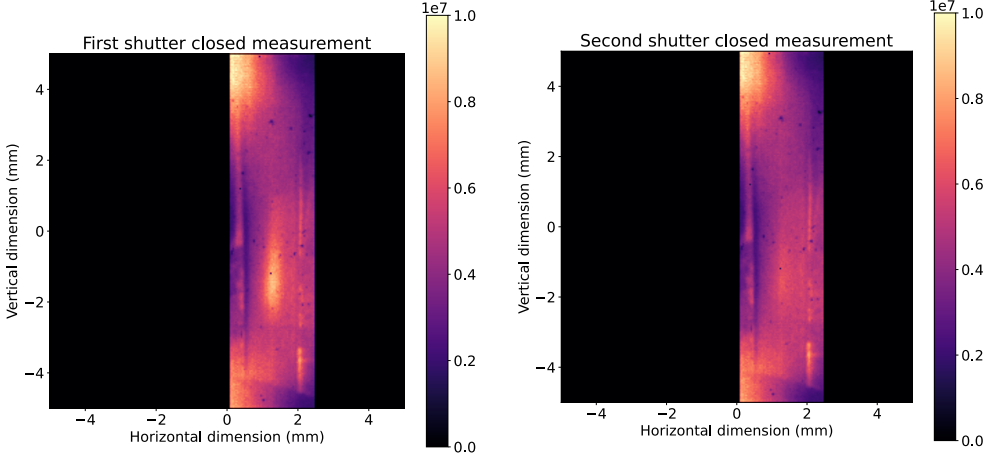


Figure 5 Images recorded after closing the shutter taken 2 minutes apart. Same color scale used. Note decay of afterglow from left to right figure. The spots on upper and lower edges arise from scattering of ambient light from the tape holding the Cd mask on the scintillator. The vertical streaks on either side of the afterglow arise from ambient light scattering from the edges of the Cd mask.

the afterglow, i.e., the residual fluorescence, and explains the offset of the camera data with respect the ${}^3\text{He}$ detector data in Figure 3 (right).

The impact of the afterglow on the reflectivity of the camera data is dramatic. The impact can be demonstrated by convoluting the reflectivity vs. time-of-flight as measured by the ${}^3\text{He}$ detector with an exponential decay function. Specifically, the reflectivity corresponding to a time-of-flight, t_0 , is the integral of the preceding reflectivities for times-of-flight ranging from $t_0 - \frac{1}{60} \text{ s}$. In principle, every period of the source prior to the period containing t_0 , also contributes through a factor that goes as $\sim \frac{1}{1-e^{-t/\tau}}$, where t and τ are time-of-flight (plus source period), i.e., absolute time, and the time constant of the decay, respectively. The result of the calculation is shown in Figure 6 for various time constants. The solid black and red curves correspond to the reflectivities measured by the ${}^3\text{He}$ detector and camera, respectively. Comparing the camera data to the convolutions vs τ , the decay time of the afterglow is likely between 1 and 10 ms and not as large as suggested by the shutter closed measurements (102 s). From Figure 6 we can also conclude that the (quadrature) sum of scintillation and afterglow decay constants as large as 10 μs is tolerable.

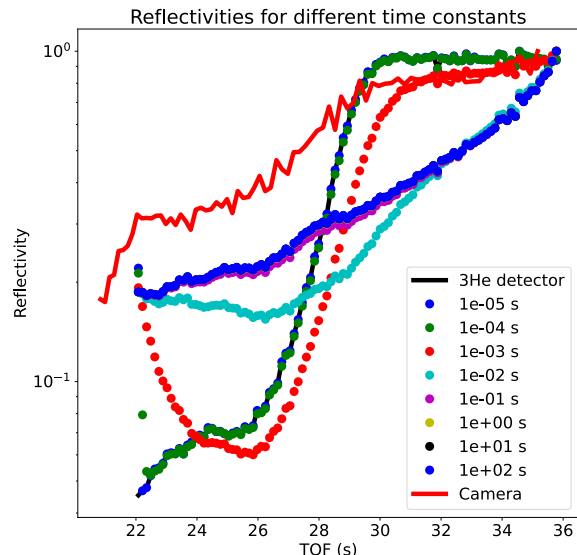


Figure 6 Using the reflectivity measured by the ${}^3\text{He}$ detector (black curve) as ideal, the impact of various decay time constants on the reflectivity. The red curve is the reflectivity measured by the camera.

Next steps

The most important next step is to identify whether a scintillator:phosphor combination exists with the sensitivity of at least the sensitivity of the LiF scintillator used here coupled to a much faster phosphor.^{‡‡} The time constant of the combination should not exceed 10 μs . The neutron to photon conversion efficiency of the combination might be improved by depositing the material on a mirrorlike surface that reflects light well in the blue. If a suitable material can be obtained, then the challenges become mere technical (IT) problems (data storage and calculation). Then, thought should be given to the opportunities afforded by a technology that has orders of magnitude better spatial resolution and speed than existing ^3He technology. For example, one can imagine placing neutron scintillators inside sample environment equipment, or in the neutron beam path along the instrument's length (e.g., for diagnostic measurements). In many instances the sample to scintillator-detector distances can be made much smaller, reducing background, e.g., air scatter, and costs, etc. Note, the focal lengths from the scintillator to the camera can be very long, if needed, without affecting the wavelength range. The ps-accuracy of the timing chips affords another opportunity; for example, hot neutron spectroscopy or MISANS for which a “thin” detector is desired.

^{‡‡} Other commercial options may be available per T. Visscher and M. Loyd.